

Fabrication of ultrahigh aspect ratio silicon nanostructures using self-assembled gold metal-assisted chemical etching

Joshua M. Duran
Andrew Sarangan

Fabrication of ultrahigh aspect ratio silicon nanostructures using self-assembled gold metal-assisted chemical etching

Joshua M. Duran^{a,b,*} and Andrew Sarangan^b

^aAir Force Research Laboratory, 2241 Avionics Circle, Wright-Patterson Air Force Base, Ohio 45433, United States

^bUniversity of Dayton, Department of Electro-Optics and Photonics, 300 College Park, Dayton, Ohio 45469, United States

Abstract. We report the critical factors that control the geometry of silicon nanostructures produced by metal-assisted chemical etching (MacEtch) using self-assembled islands from an ultrathin film of gold. We have conducted a systematic study of the process parameters that control the geometry of the metal structures and the resulting etched nanostructures. Compared to prior reports, which have focused on the crystal orientation and solution stoichiometry, our study finds that the anisotropy of the etched nanostructures is primarily controlled by the deposited metal geometry, while solution stoichiometry and crystal orientation play relatively minor roles. Using an optimized self-assembled geometry and etch process, we demonstrate what we believe is the highest aspect ratio to date (greater than 5000:1) for high density top-down etched silicon nanostructures. These structures, which we refer to as silicon nanowalls, are in the size regime where quantum confinement effects could potentially be exploited for next-generation optoelectronic components and devices. © The Authors. Published by SPIE under a Creative Commons Attribution 3.0 Unported License. Distribution or reproduction of this work in whole or in part requires full attribution of the original publication, including its DOI. [DOI: [10.1117/1.JMM.16.1.014502](https://doi.org/10.1117/1.JMM.16.1.014502)]

Keywords: MacEtch; MACE; metal assisted chemical etching; quantum walls; nanostructures; nanowires; nanowalls; nanosheets; high-aspect ratio etching.

Paper 16149 received Oct. 11, 2016; accepted for publication Jan. 6, 2017; published online Feb. 1, 2017.

1 Introduction

Nanostructured semiconductors have received significant attention over the past decade because of their potential to alter the optical and electrical properties from bulk crystalline values. While this concept is widely exploited in III-V semiconductors,¹ silicon has been more challenging because of a lack of suitable materials with the proper band structure and lattice. Nevertheless, alternate ways of engineering the band structure of silicon could expand its utility in future applications where bulk crystalline silicon is not suitable. The bottom-up approach to growing silicon nanowires has been extensively studied,² but a top-down approach from a single crystal silicon substrate would be more practical for near-term device exploitation. One such approach leverages a technique known as metal-assisted chemical etching (MacEtch). MacEtch relies on the galvanic corrosion of silicon in the presence of a noble metal (catalyst) to provide a dramatic etch contrast in a wet chemical solution containing hydrofluoric (HF) acid and an oxidizing agent (typically H₂O₂ or HNO₃).^{3–5} Unlike most conventional wet/dry etch processes that require an etch mask to define features, MacEtch uses a metal template as an etch-promoter. In this process, silicon in direct contact with metal etches away leaving behind silicon structures in the voids between the metal patterns, as illustrated in Fig. 1. It has been reported previously that the remaining silicon structures can be crystalline or porous in nature depending on the etchant solution stoichiometry, substrate doping, and metal catalyst type.^{6–10}

MacEtch has been demonstrated on lithographically patterned^{6,11,12} and self-assembled metal patterns.^{4,5,7,8,13–15}

With self-assembly, it is possible to reach geometrical features far smaller than what can be realized by lithographic patterning. The most common self-assembly approach uses a metal salt bath, such as AgNO₃,^{8,9,14,16–18} where the etch geometry is defined by silver dendrite formation from the solution. While modest control of the dendrite geometry has been demonstrated,¹⁸ the resulting etched features are larger than 50 nm. Generally, features smaller than 10 nm are necessary to observe quantum confinement effects.¹⁹ Therefore, in this work, we have focused on developing methods to create self-assembled metal structures smaller than 10 nm.¹⁵

One method for forming self-assembled metal patterns smaller than 10 nm is by depositing an ultrathin metal film using physical vapor deposition (PVD) and controlling the thickness near its percolation threshold. It is well known that metal films deposited onto (semi)insulating substrates evolve to a thin-film state via a morphological sequence: it initially forms compact islands, then elongated islands, percolation, hole filling, and finally the thin-film state.²⁰ By precise control of film thickness, we have been able to utilize the metal patterns of this morphological sequence as the catalyst for the MacEtch process. This is more attractive compared to metal salt baths because PVD deposition is widely available with greater uniformity, low cost, and ultrahigh purity. The focus of this paper is the fabrication process for MacEtch of silicon nanostructures with lateral features smaller than 10 nm using PVD patterned gold.

2 Experimental Results and Discussion

All experiments reported in this paper were done using moderately boron-doped silicon substrates with bulk resistivity values in the range of 1 to 100 Ω • cm. Overall, the process

*Address all correspondence to: Joshua M. Duran, E-mail: joshua.duran.2@us.af.mil

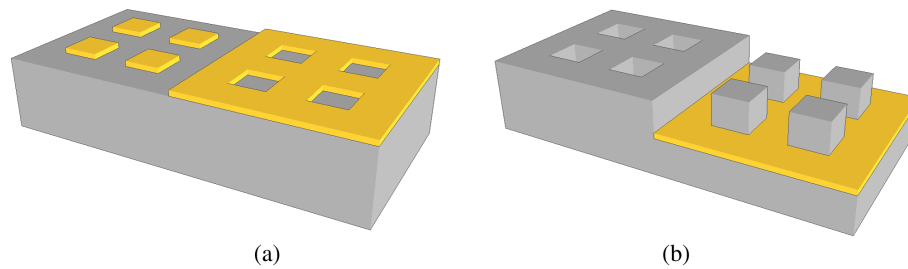


Fig. 1 Illustration depicting the profile view of MacEtch fabrication process: (a) metal pattern on silicon before MacEtch and (b) resulting silicon nanostructures after MacEtch.

steps consisted of an initial oxide etch/clean in a buffered oxide etch (BOE) solution, controlled reoxidation in an oxygen plasma, PVD metal deposition, MacEtch in a HF + H₂O₂ bath, critical point drying, and inspection. Each of these processes is discussed in greater detail in the following sections.

2.1 Substrate Preparation

While MacEtch has been shown to work with a variety of metals,^{3,14} our work focuses on gold for several reasons: silver has been studied most extensively, but its percolation threshold is relatively thick and the resulting self-assembled structures subsequently form features much larger than 10 nm. Silver also has the undesirable characteristic of etching slowly in H₂O₂;⁷ this can lead to imperfect pattern reproduction as the silver pattern dissolves in the etching solution. Some other metals, such as platinum and palladium, are known to leave behind porously etched silicon rather than preserving the crystalline nature.^{10,21} In comparison, gold produces smaller self-assembled features, is resilient to the etching solution, and preserves the crystalline nature of the remaining silicon structures.

Our results point to two primary factors that affect the morphological sequence of PVD metal patterns for a given substrate and a given metal: (1) the nature of the native oxide on the surface and (2) substrate temperature during deposition. The first parameter plays a crucial role in how the metal nucleates and grows on the surface. Stripping the native oxide layer with a BOE solution immediately

prior to the sputtered gold deposition resulted in continuous films for films as thin as 2 nm at room temperature (i.e., they had ultrathin percolation thresholds). Such ultrathin gold films were found to be nearly impossible to remove in a wet etchant, suggesting the formation of a silicide at room temperatures. Furthermore, films thinner than 2 nm are not easily controllable or reproducible due to the extremely short deposition times, therefore oxide-free silicon is not ideal for forming the desired gold patterns. To create a controllable and repeatable oxidized silicon substrate, first, the native oxide was stripped for 30 s in a BOE solution. A standard 6:1 BOE solution was used with a volume ratio of 40% NH₄F (in water) to 49% HF (in water), and further diluted 1:10 BOE:DI water. The wafers were then immediately reoxidized in an oxygen barrel plasma asher (LFE Systems 110) for 2 min at 200 W and 100 mTorr. Compared to an ambient native oxide, this allowed us to form a reproducible oxide prior to each metal deposition. An example of the self-assembled structures with and without substrate oxidation is shown in Fig. 2.

2.2 Physical Vapor Deposition Metal Deposition

Depositions were done using a Denton Discovery 18 RF sputter deposition tool. Because ultrathin films do not immediately form a continuous layer, there is an inherent ambiguity in defining the layer thickness. Our approach is to first deposit a film thick enough to form a continuous layer that can be measured with a profilometer. The deposition rate is then calculated assuming a constant rate over the

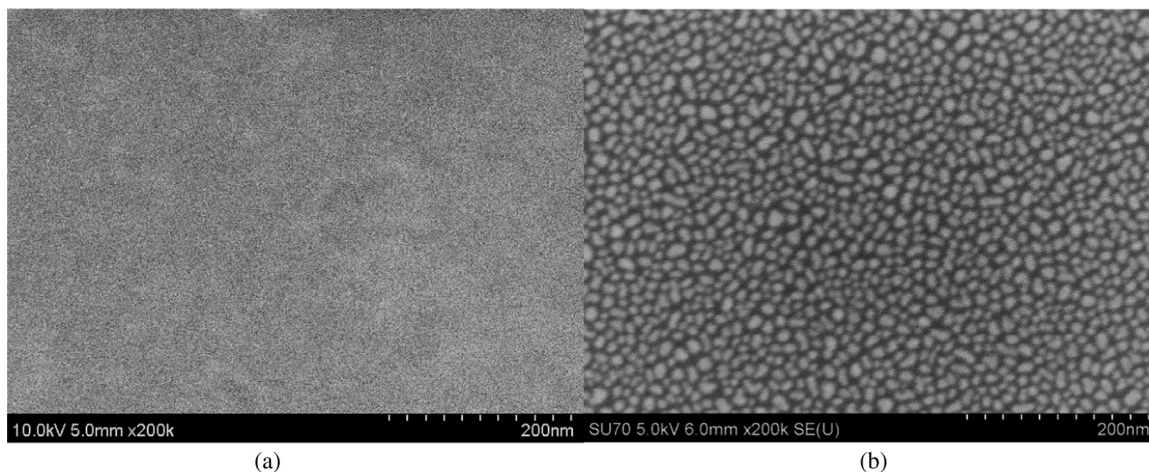


Fig. 2 SEM images of 2-nm sputtered gold on (a) BOE etched silicon (without an oxide) and (b) intentionally oxidized silicon using an oxygen plasma. Both images are shown at the same scale to highlight the difference.

full deposition time window (calculated from a number of different deposition thicknesses). The film “thickness” we report is simply this calibrated rate multiplied by the deposition time. Due to the evolution of the morphological sequence, this thickness should be treated as an average extrapolated thickness rather than the height of the film at any given position on the substrate. We feel this distinction is irrelevant because the definition of thickness of discontinuous metal films itself is ambiguous. The substrates were loaded into the vacuum chamber and pumped down to a base pressure below $1\text{E-}6$ Torr. The deposition process pressure was 2.5 mTorr with 100-W RF power. Each deposition included a 1 min presputter for target conditioning, with a previously calibrated deposition rate of 5 \AA/s . After the deposition, the metal pattern on the substrates was examined using a Hitachi SU-70 SEM tool. For the MacEtch process, we found that the geometry of the resulting metal traces is a reliable indicator of thickness compared to other metrology techniques.

In addition to the role of surface oxide as discussed previously, the second important process parameter is the substrate temperature during deposition. We found that increasing the substrate temperature increased the percolation threshold, and therefore, increased the sizes of the self-assembled structures. This is shown in Fig. 3, where two samples feature metal morphologies near the percolation threshold of the film, but the 200°C growth requires a significantly thicker metal deposition relative to the room temperature deposition to reach the same phase of the morphology evolution. It is interesting to note that while, overall, the Au pattern size increases for a heated substrate, within the parameter space we examined the size of the metal features appear to increase relatively more than the gaps between the metal pattern. This also leads us to believe that a smaller percolation threshold could be achieved by cooling the substrate,²² but this was not studied in this work.

2.3 MacEtch Process

In order to utilize the metal patterns to achieve high-density silicon nanostructures, etching must progress perfectly vertical to the surface, i.e., the etch must be highly anisotropic. Even a slight rate of undercut would limit the maximum

depth that could be achieved and cause structures to collapse; the density of the nanostructures could also dramatically decrease as many of the structures would be lifted off due to the undercut. While MacEtch is known to have a crystalline dependency,^{6,7,9,17} the role of solution ratio has conflicting reports^{4,6,7,9,12} and the role of metal geometry has not been studied extensively.^{5,12} Furthermore, it should also be noted that previous studies have generally been limited to metal patterns that are significantly larger than the patterns we have examined.^{5-9,12,13,16-18} To test the impact of solution ratio, we performed the etch at six different ratios (by volume): 6:1, 3:1, 2:1, 3:2, 1:1, and 1:2 HF:H₂O₂ for 1 min. This grouping of ratios straddles what was reported by Chartier et al.⁴ to be the optimal concentration of 80% HF to 20% H₂O₂ by mol corresponding to a volumetric ratio of nearly 3:2 for maximum metal penetration rate. Solutions were composed of 60 mL HF with the appropriate amount of H₂O₂ added based on the desired ratio. Because of this, the high HF concentration solutions were a smaller total volume than the low HF solutions. We do not believe that the solution volume plays a significant role in the etch process so long as the sample size is much smaller than the solution volume.

Etchant solutions were formulated from 49% HF (in water) and 30% H₂O₂ (in water). The HF was added to H₂O₂ and manually stirred for 20 s prior to etching. Etchant solutions were used for multiple trials but were replaced after a maximum of 5 days of use; no noticeable degradation of the solution was observed over this timeframe as indicated by consistent etch rates for identical samples that were etched days apart. To minimize the impact of evaporation on the solution stoichiometry due to significant differences in the vapor pressure of the constituents, solutions were kept in a sealed container whenever not in use. Metal deposition was performed on 3-in. wafers and cleaved into square shapes approximately 2 to 3 cm in each dimension. This way, metal patterns from a single deposition cycle could be etched in several solutions and be compared directly. Samples were held with a plastic clamping tool and dipped into the solution for 1 min. After the etch, the sample was immediately transferred to a DI water bath for rinsing for another minute. While measurements of the

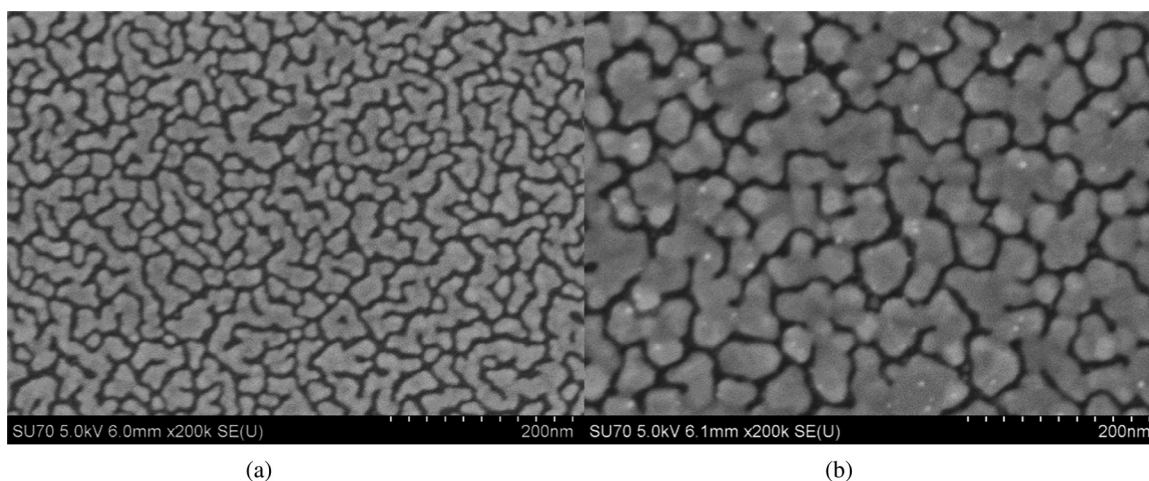


Fig. 3 SEM images of (a) 4-nm thick gold film at room temperature and (b) 16-nm gold film at 200°C , both on oxidized silicon substrate. Both images are shown at the same scale.

uniformity of the etch were not performed for these samples, no significant visual nonuniformity was observed during or after the etch process apart from sparse circular shapes due to H_2 bubble formation during the etch. Bubbles have been reported to cause localized etch nonuniformity²³ and we observed the same effect. These areas were avoided for SEM evaluation of the samples by cleaving in regions not impacted by bubble formation on the sample. During SEM imaging of the etch profile, care was taken to inspect several distant locations on the sample to qualitatively verify the uniformity and ensure that the images used were representative of the sample as a whole. None of the samples etched during this experiment showed significant differences in the etch profile across the sample.

Figure 4 shows the summary of results from two different self-assembled metal geometries on $\langle 100 \rangle$ and $\langle 111 \rangle$ substrates. The result indicates a strong dependence of the etch anisotropy on the metal pattern geometry. The etch anisotropy appears to be only weakly dependent on the solution chemistry and crystal orientation. The most noticeable aspect is that small isolated metal islands etch in generally

unpredictable directions while larger islands and interconnected web-like patterns etch nearly perpendicular to the surface. This effect was also observed by Romano et al.²³ while investigating the suitability of porous gold films for micro-machining silicon.

2.4 Characterization of the MacEtch Process

To quantify the anisotropy of the etch results of over 30 trials, we have computationally analyzed the SEM images with respect to the original metal feature sizes, MacEtch solution stoichiometry, and substrate crystal orientation. All of these samples were etched for 1 min according to the procedure outlined in the previous section. Top view SEM images of the metal patterns were passed through a Gaussian filter and subsequently segmented using thresholding in order to calculate the average area of the metal features responsible for the etch, as shown in Fig. 5. Area was calculated by summing the segmented pixels and converting to an area using the scale bar of the SEM image (200k zoom used for all images). Cross-sectional profile images after the MacEtch

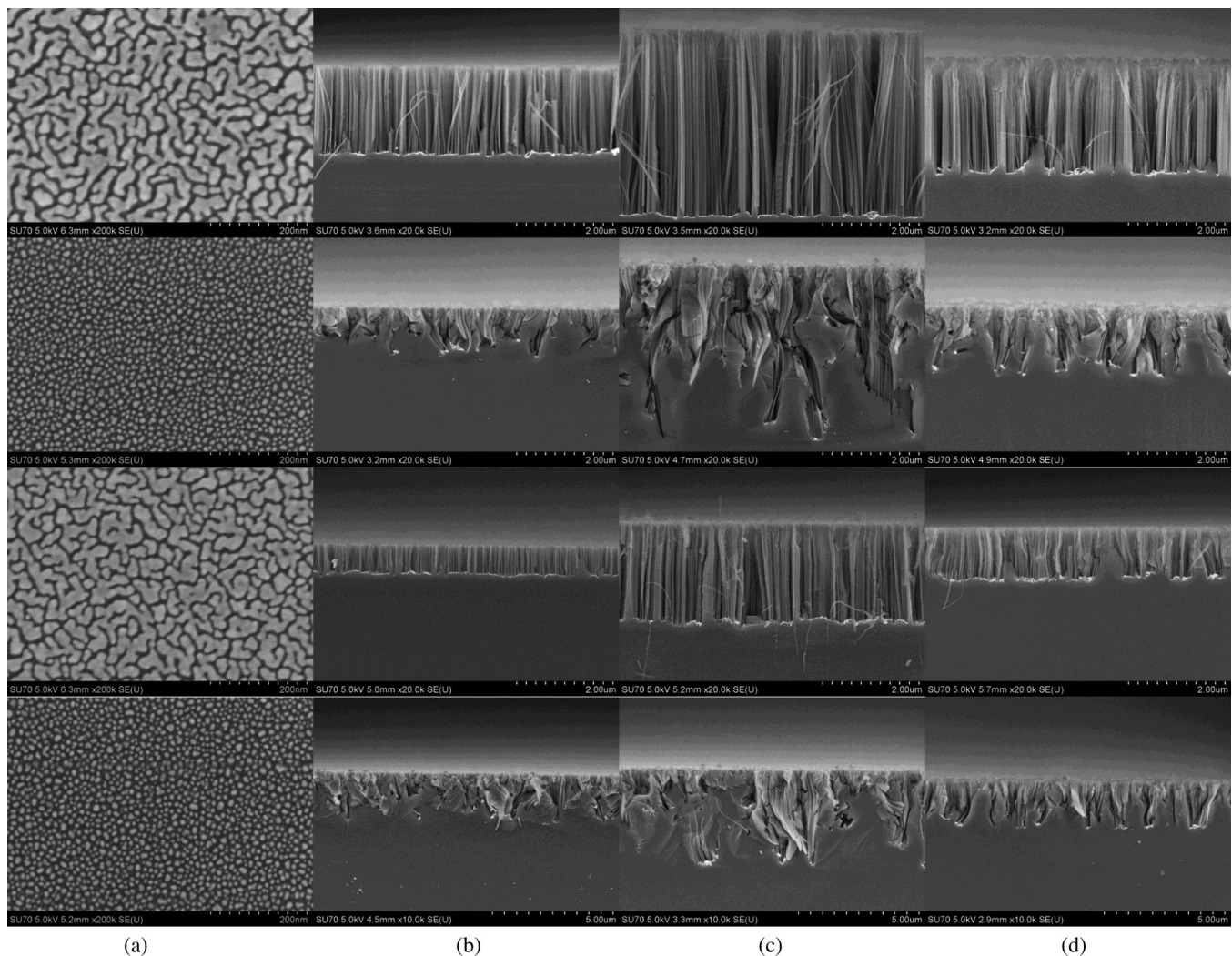


Fig. 4 Comparison of metal pattern geometry, substrate crystal orientation, and solution stoichiometry on etch profile. (Column a) Gold pattern for room temperature depositions of 4 nm (large particles) and 2 nm (small particles), (column b) 6:1 HF:H₂O₂, (column c) 3:2 HF:H₂O₂, (column d) 1:2 HF:H₂O₂, (rows 1 and 2) on $\langle 100 \rangle$ wafers and (rows 3 and 4) on $\langle 111 \rangle$ wafers. Etch duration was 60 s in all cases.

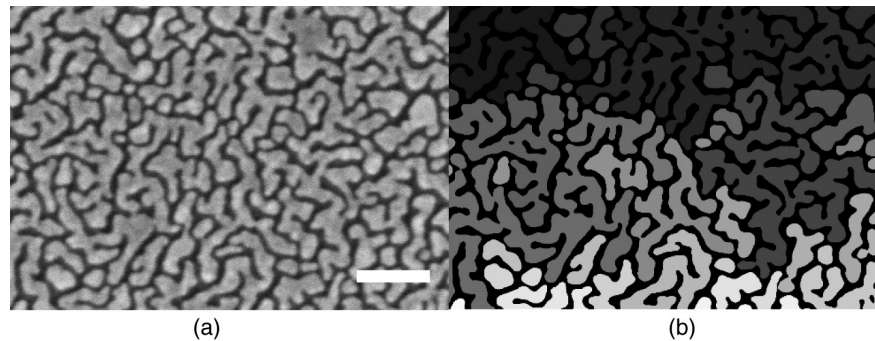


Fig. 5 Example of (a) original metal pattern and (b) segmented image of metal pattern; each shade represents an isolated particle. This sample is a room temperature deposition of 4-nm gold. Scale bar is 100 nm.

were used to characterize the etch anisotropy. Because we fixed the etch duration, etch depth varied with solution stoichiometry. To accommodate this, SEM profile images of identical zoom (20k) were cropped to only include the etched features for analysis. All computational analyses on the SEM images were done using open-source Python and associated packages including Numpy,²⁴ Matplotlib,²⁵ and scikit-image.²⁶

To determine the direction of the etch, first, a canny edge detection technique was used on cropped images to extract the edge pixels from the image. A 2-D correlation between the edge image and a horizontal, vertical, and ± 45 deg structuring element was performed at each edge pixel; the strongest correlation value among those calculations was used to define the approximate angle of the etch at that location. The mean of the angles at all pixels along the etch edges was then calculated to define the average angle of etch for each experimental result. This is shown in Fig. 6. All processed images were manually inspected after the process to verify the integrity of the calculated results. Accurate metal pattern segmentation required manual adjustment of the thresholding level for each pattern, while the automated edge detection and etch angle analysis produced reliable results without manual intervention.

The computed results are shown in Fig. 7. This analysis is not infallible due to the imperfect nature of the SEM images used for the analysis. The drying/cleaving and sample preparation process often results in the collapse of some nanostructures near the cleaved edges that are not representative of the actual etch direction; these results are, therefore, meant to

serve as an experimental guide to indicate the overall behavioral trends under the conditions tested.

As mentioned earlier, Fig. 7 does not show a strong dependence of etch anisotropy on the solution stoichiometry or crystal orientation. It is clear, however, that etched structures from medium to large metal patterns (represented by medium to large markers in Fig. 7) etch fairly normal to the surface, while small isolated islands do not. We attribute this behavior to the increased influence of momentum transfer for smaller particles from expelled gaseous byproducts from the etch process. As the particle size and surface contact area decrease, the forces imparted by these byproducts begin to compete with van der Waals forces that keep the metal particle in contact with the substrate.²⁷

The data in Fig. 8 numerically show a threshold size requirement for achieving highly anisotropic etching. Particles with a footprint greater than ~ 100 nm² etch anisotropically while particles with a smaller footprint do not. This threshold value is also a function of the contact area of the metal features; in separately conducted experimental trials, we found that commercially available 50-nm colloidal gold nanoparticles did not etch vertically despite their relatively large size. This is because the contact area (and hence van der Waals force) of a colloidal nanoparticle is much smaller than the flattened pancake-shaped features formed by PVD islands.²⁸ It should be noted that all metal patterns used in these etch trials feature voids (i.e., do not form a continuous film) to limit the effect of hole diffusion process on the etch. It is known that MacEtch does not progress for large-area void-free metal catalysts,¹¹ so metal patterns of

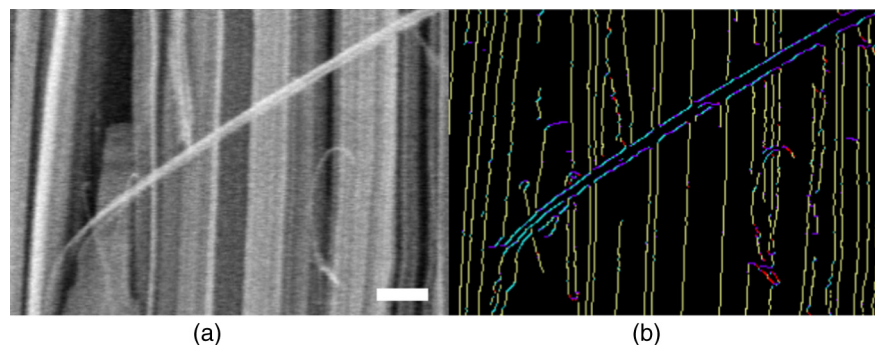


Fig. 6 High resolution cropped view of (a) original etch profile and (b) image after edge detection and angle determination (colors represent 0, 90, ± 45 deg angles). This etch profile is from the same sample used in Fig. 5 etched using a 1:1 HF:H₂O₂ volume ratio. Scale bar is 200 nm.

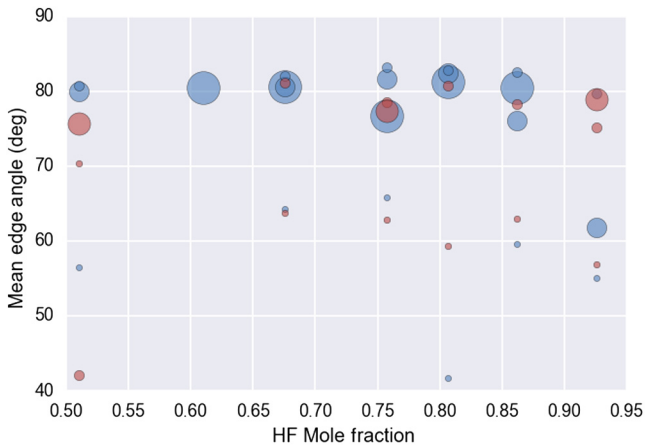


Fig. 7 Plot of etch anisotropy for numerous etch trials. Blue markers represent $\langle 100 \rangle$ wafers, red represent $\langle 111 \rangle$. The size of the markers is proportional to the mean size of the metal particles on the substrate.

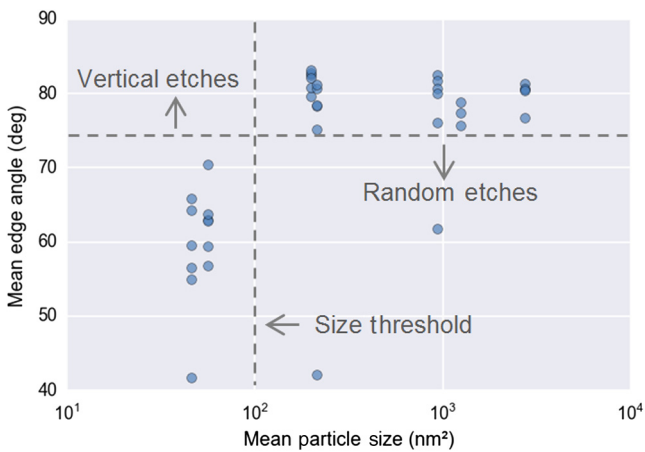


Fig. 8 Summary plot of numerous etch trials highlighting size dependence.

this type were not investigated. The plot in Fig. 8 contains two etch trials with relatively large metal footprints that did not etch vertically, which merits further discussion. One of these samples was a metal pattern on a $\langle 100 \rangle$ wafer etched in

a high HF concentration solution (6:1) while the other was on a $\langle 111 \rangle$ wafer etched in low HF concentration solution (1:2). This data is in agreement with Chern et al.,⁶ who suggest the formation of slanted etched profiles of $\langle 100 \rangle$ wafers for high HF concentration solutions as well for $\langle 111 \rangle$ wafers with low HF concentration solutions. Because these two samples were the only two which appeared to be influenced primarily by the solution stoichiometry rather than metal pattern morphology, we conclude that the pattern morphology is the primary influence over etch direction for the metal pattern size regime and solution stoichiometry tested; while a secondary influence can be attributed to solution stoichiometry, particularly at the extreme ends of the solution ratios tested.

2.5 Ultrahigh Aspect Ratio MacEtch Processing

Based on our experiments, the optimized process for producing highly anisotropic etching of ultra-fine silicon nanostructures is an interconnected gold pattern on an oxidized $\langle 100 \rangle$ silicon wafer, as shown in Fig. 3(a). From a large number of etch trials, the optimized etch solution was found to be 3:2 HF:H₂O₂ to produce a nearly perfect anisotropy as well as a high etch rate. To further confirm this optimized process, a much longer (8 min) etch was conducted, for which even a small deviation from a perfect anisotropy would lead to significant undercutting and a loss of nanowires.

The results from this longer etch are shown in Fig. 9. From the SEM cross-sectional view [Fig. 9(b)], we observe nearly ideal anisotropy indicated by the high density of nanostructures and vertical etch profiles. To obtain an estimate of the aspect ratio, first, we reference the original metal pattern; this pattern is transferred faithfully to the silicon substrate such that the average space between metal patterns is equal to the average silicon nanostructure width. This was verified using a shorter etch time to more easily observe the direct pattern transfer shown in Fig. 10. From Fig. 10(c), we can see the metal trace lying at the bottom of the etched trenches almost unchanged in shape.

The original mesh-like metal structure translates into the silicon to create vertically standing walls of silicon sheets (nanowalls). The width of the void areas in the metal traces varies between 5 and 10 nm while the meandering length of

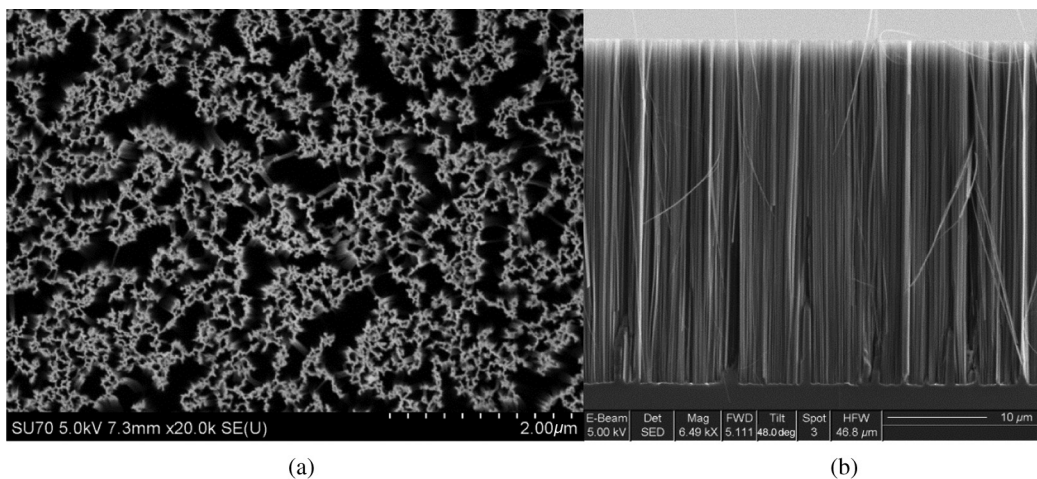


Fig. 9 SEM images of silicon nanostructures from (a) top and (b) side views using optimized 8 min MacEtch process with 5-nm Au film deposited at room temperature.

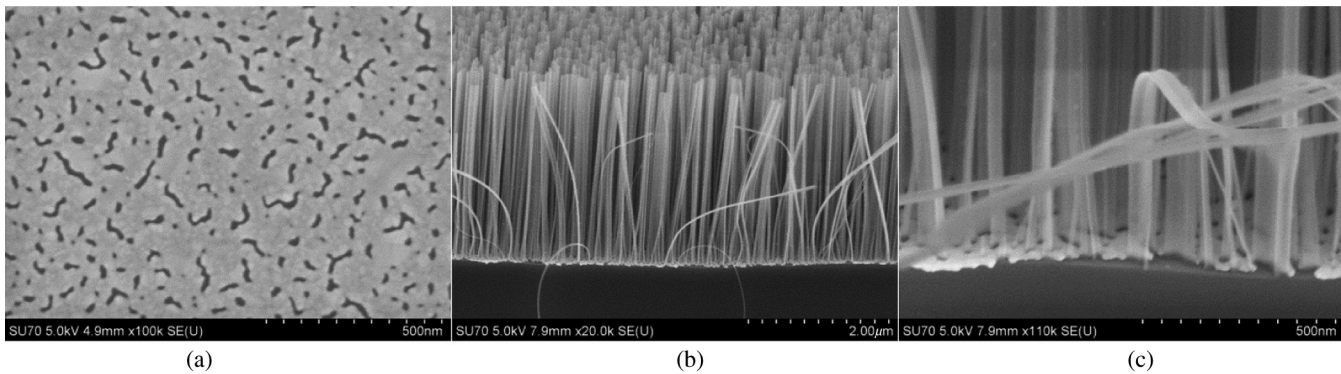


Fig. 10 Etch process demonstrating a faithful pattern transfer: (a) original 5-nm room temperature deposited metal pattern, (b) $\frac{3}{4}$ view postetch, and (c) close-up detail highlighting ideal pattern transfer.

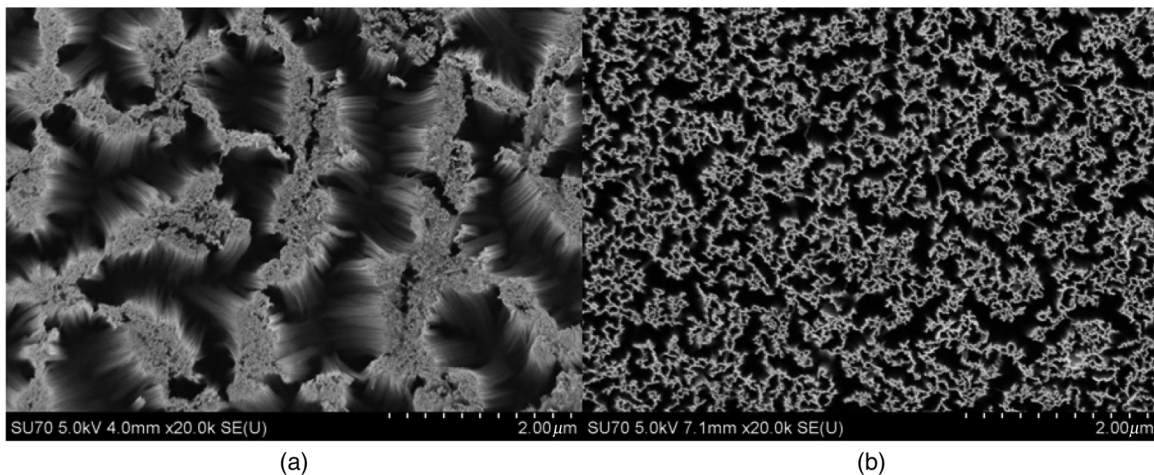


Fig. 11 Top view SEM images of Si nanostructures that have been dried using (a) a nitrogen blow gun and (b) CPD process. A 5-nm room temperature Au deposition was used as the metal catalyst in a 3:2 HF:H₂O₂ solution etch for 1 min.

these voids can be several hundred nanometers. These numbers are verified after the etch using a side-view SEM image. The nanowall height is defined by the etch depth and was measured to be $36\ \mu\text{m}$ for the 8-min etch. The resulting structures have an impressive aspect ratio as high as 7200:1. To our knowledge, this is the largest aspect ratio achieved by a top-down fabrication of high-density structures, by a significant margin.⁸ It should be noted that the etch process was arbitrarily terminated after 8 min; it is likely that even higher aspect ratios are possible simply by continuing this procedure for longer durations.

It is also important to point out that the drying process used immediately after the wet MacEtch and rinse plays a crucial role in the survivability of these nanostructures. Due to the capillary forces during the drying process, air or nitrogen dried samples produced severely collapsed or bunched-up features. As a result, we utilized a CO₂ critical-point drying (CPD) technique, especially for the high-aspect ratio structures. This is a standard technique used to overcome the structural collapse during drying and is widely used in MEMS devices. Figure 11 shows the resulting structures with and without the CPD process.

2.6 Summary and Conclusions

In summary, we have demonstrated a low-cost fabrication method for producing sub-10 nm silicon nanostructures using

self-assembled metal patterns from ultrathin films produced by PVD. The patterns were produced by controlling the film thickness near their percolation threshold. Substrate temperature and the presence of a surface oxide were the primary factors that influence the geometry of the resulting metal structures. Our results indicate that the geometry of the metal structure is the most important factor that determines the etch anisotropy, compared to other factors such as crystal orientation or solution stoichiometry. Larger islands or mesh-like interconnected shapes exhibit a greater anisotropy than isolated small particles, and small spherical nanoparticles were not found to etch anisotropically. Of all the metals we examined, gold was chosen to be the most suitable for creating 5 to 10 nm high aspect ratio structures. The resulting silicon nanostructures, which we refer to as silicon nanowalls, are extremely low cost and relatively easy to fabricate using standard semiconductor fabrication tooling and chemicals. These unique features make these structures an exciting prospect for next-generation silicon-based quantum-engineered optoelectronic components and devices.

Acknowledgments

This work was funded by the Entrepreneurial Research Fund through the Air Force Research Laboratory. The authors declare no conflicts of interest related to the publishing of this content.

References

1. B. F. Levine, "Quantum-well infrared photodetectors," *J. Appl. Phys.* **74**(8), R1–R81 (1993).
2. H. J. Fan, P. Werner, and M. Zacharias, "Semiconductor nanowires: from self-organization to patterned growth," *Small* **2**(6), 700–717 (2006).
3. X. Li and P. W. Bohn, "Metal-assisted chemical etching in HF/H₂O₂ produces porous silicon," *Appl. Phys. Lett.* **77**(16), 2572–2574 (2000).
4. C. Chartier, S. Bastide, and C. Levy-Clement, "Metal-assisted chemical etching of silicon in HF-H₂O₂," *Electrochim. Acta* **53**(17), 5509–5516 (2008).
5. C.-L. Lee et al., "Pore formation in silicon by wet etching using micrometre-sized metal particles as catalysts," *J. Mater. Chem.* **18**(9), 1015–1020 (2008).
6. W. Chem et al., "Nonlithographic patterning and metal-assisted chemical etching for manufacturing of tunable light-emitting silicon nanowire arrays," *Nano Lett.* **10**(5), 1582–1588 (2010).
7. J. Kim et al., "Au/Ag bilayered metal mesh as a Si etching catalyst for controlled fabrication of Si nanowires," *ACS Nano* **5**(4), 3222–3229 (2011).
8. M.-L. Zhang et al., "Preparation of large-area uniform silicon nanowires arrays through metal-assisted chemical etching," *J. Phys. Chem. C* **112**(12), 4444–4450 (2008).
9. Z. Huang et al., "Oxidation rate effect on the direction of metal-assisted chemical and electrochemical etching of silicon," *J. Phys. Chem. C* **114**(24), 10683–10690 (2010).
10. X. P. Li et al., "Influence of the mobility of Pt nanoparticles on the anisotropic etching properties of silicon," *ECS Solid State Lett.* **2**(2), P22–P24 (2013).
11. M. Zahedinejad et al., "Deep and vertical silicon bulk micromachining using metal assisted chemical etching," *J. Micromech. Microeng.* **23**(5), 055015 (2013).
12. O. J. Hildreth, W. Lin, and C. P. Wong, "Effect of catalyst shape and etchant composition on etching direction in metal-assisted chemical etching of silicon to fabricate 3D nanostructures," *ACS Nano* **3**(12), 4033–4042 (2009).
13. S. P. Scheeler et al., "Fabrication of porous silicon by metal-assisted etching using highly ordered gold nanoparticle arrays," *Nanoscale Res. Lett.* **7**, 450 (2012).
14. S. Yae et al., "Catalytic activity of noble metals for metal-assisted chemical etching of silicon," *Nanoscale Res. Lett.* **7**, 352 (2012).
15. Z. Huang et al., "Extended arrays of vertically aligned sub-10 nm diameter 100 Si nanowires by metal-assisted chemical etching," *Nano Lett.* **8**(9), 3046–3051 (2008).
16. Y. Qu et al., "Electrically conductive and optically active porous silicon nanowires," *Nano Lett.* **9**(12), 4539–4543 (2009).
17. H. Chen et al., "Wafer-scale synthesis of single-crystal zigzag silicon nanowire arrays with controlled turning angles," *Nano Lett.* **10**(3), 864–868 (2010).
18. C.-Y. Chen et al., "Morphological control of single-crystalline silicon nanowire arrays near room temperature," *Adv. Mater.* **20**(20), 3811–3815 (2008).
19. F. A. Zwanenburg et al., "Silicon quantum electronics," *Rev. Mod. Phys.* **85**(3), 961–1019 (2013).
20. X. Yu et al., "Coalescence and percolation in thin metal-films," *Phys. Rev. B* **44**(23), 13163–13166 (1991).
21. S. Chattopadhyay, X. L. Li, and P. W. Bohn, "In-plane control of morphology and tunable photoluminescence in porous silicon produced by metal-assisted electroless chemical etching," *J. Appl. Phys.* **91**(9), 6134–6140 (2002).
22. P. J. Shah, X. Niu, and A. Sarangan, "High aspect ratio silver nanorod thin films grown at cryogenic substrate temperature," *J. Nanosci. Lett.* **3**, 19 (2013).
23. L. Romano et al., "Self-assembly nanostructured gold for high aspect ratio silicon microstructures by metal assisted chemical etching," *RSC Adv.* **6**(19), 16025–16029 (2016).
24. S. van der Walt, S. C. Colbert, and G. Varoquaux, "The NumPy array: a structure for efficient numerical computation," *Comput. Sci. Eng.* **13**(2), 22–30 (2011).
25. J. D. Hunter, "Matplotlib: a 2D graphics environment," *Comput. Sci. Eng.* **9**(3), 90–95 (2007).
26. S. van der Walt et al., "Scikit-image: image processing in Python," *PeerJ* **2**, e453 (2014).
27. C. Q. Lai et al., "Mechanics of catalyst motion during metal assisted chemical etching of silicon," *J. Phys. Chem. C* **117**(40), 20802–20809 (2013).
28. J. Bardeen, "The image and van der Waals forces at a metallic surface," *Phys. Rev.* **58**(8), 727–736 (1940).

Joshua M. Duran received his BS degree in engineering physics from the University of Wisconsin—Platteville in 2008 and his MS degree from the University of Dayton in electro-optics engineering in 2011. He is a research electronics engineer for the Air Force Research Laboratory (sensors directorate) focused on research and development of infrared photodetectors and focal plane arrays.

Andrew Sarangan received his BAsC and PhD degrees from the University of Waterloo in Canada in 1991 and 1997, respectively. He is a professor in the Department of Electro Optics and Photonics at the University of Dayton, Ohio, USA. His current work includes novel concepts in photodetection, image sensors, optical thin films, and nanolithography. He has built and maintains a single-PI nanofabrication cleanroom.